A_3Tt_5 Phases Sr_3Sn_5, Ba_3Pb_5, and La_3Sn_5. Structure and Bonding in a Series of Isotypic Metallic Compounds with Increased Electron Count and Their Comparison with the Nominal Zintl Phase La_3In_5

Michael T. Klem, J. T. Vaughey, Jason G. Harp, and John D. Corbett*

Department of Chemistry and Ames Laboratory—DOE,[1] Iowa State University, Ames, Iowa 50011

Received July 27, 2001

A series of compounds that contain square pyramidal Tt_5 polyanions of tin and lead has been obtained in alkaline-earth or rare-earth metal−tetrel systems by direct fusion of the elements at 570 °C (Sr_3Sn_5), 1000 °C (Ba_3Pb_5), or 1300 °C (La_3Sn_5) followed by slow cooling or annealing. The crystal structures for all three have been refined in the Pu_3Pd_5 structure type (orthorhombic, *Cmcm*, $Z = 4$) with cell dimensions of $a = 10.644(2)$, 11.154(7), and 10.352(5) Å, $b = 8.588(1)$, 9.049(7), and 8.290(6) Å, and $c = 10.895(2)$, 11.370(5), and 10.652(5) Å for Sr_3Sn_5, Ba_3Pb_5, and La_3Sn_5, respectively. Square pyramidal clusters of the tetrel elements are weakly interlinked into chains via two types of longer intercluster interactions that are mediated by bridging cations and substantially influenced by cation size and the free electron count. The new compounds are all metallic ($\rho_{295} \sim 10$ (Sr_3Sn_5) to ~ 25 (La_3Sn_5) $\mu\Omega$·cm), in agreement with simple valence considerations that predict two and five extra electrons per formula unit, respectively, beyond that necessary for closed-shell *nido*-Tt_5^{4-} anions. Extended Hückel tight-binding calculations on the new compounds as well as on La_3In_5 reveal that bonding in the regions below and around the Fermi energies are dominated by general cation−anion interactions, that is, lattice covalency. Closed-shell bonding features for the classical Sn_5^{4-}, In_5^{9-}, etc. ions are also obvious but subsidiary to the heteroatomic interactions with the cations. The intercluster contacts are relatively unimportant in bonding.

Introduction

Both Zintl−Klemm and Wade's principles are useful in inorganic chemistry because of their utility in the correlations of geometric and electronic structures and compositions.[2] Zintl's approach also has predictive power and offers insights into properties and bonding considerations for many main-group solid-state materials. Some years ago we considered this correlation between electron count and cluster geometry for two new compounds with the novel Pu_3Pd_5 structure type,[3] La_3In_5 and β-Y_3In_5,[4] in which there are chemically distinctive cluster anions of square pyramidal In_5. According to Wade's rules (or simple MO calculations), the indium square pyramids would be classified as nido deltahedra with $2n + 4$ skeletal electrons (14) and a charge of 9−, thereby matching the expected contribution from three rare-earth metal atoms and making these salts structurally Zintl phases. Although the fact that both phases are poor metals (La_3In_5: $\rho_{295} = 90\ \mu\Omega$·cm, $\chi_{Pauli} = \sim 4 \times 10^{-4}$ emu·mol^{-1}) may seem to deny their strict classification as Zintl (valence) compounds, this situation is in various degrees common at least among alkali-metal−triel systems relative to analogous compounds of later main-group elements. Diminishing band gaps and increased covalency may be important in these systems. Nonetheless, the compositions of numerous cluster compounds, and their properties when known, still encourage useful and meaningful descriptions of most of them in terms of low lying valence electron pair bonding of the post-transition components, often in clusters, that clearly reflect significant and nominally closed shells in regular and predictable patterns.[5]

The stabilities of diverse ionic cluster salts in solids are clearly often influenced by packing as well as electronic effects. Chemical modifications of the sizes of the cations or anions along with perhaps the formal charge on either can lead to new structure types, although these perhaps more often lead to instability of the cluster species. In the particular examples of the Pu_3Pd_5 structure type reported here, variations in the electron requirements of the main-group polyanions together with charges on the countercations have been found to lead to a novel series of salts in which different numbers of nominally free, metallic electrons remain beyond Tt_5^{4-} clusters, namely, $Sr_3Sn_5 + 2e^-$, $Ba_3Pb_5 + 2e^-$, and $La_3Sn_5 + 5e^-$ to add to the earlier electron-precise examples La_3In_5 and β-Y_3In_5. This structure type also raises other issues in that the limited number of countercations allow appreciable interanionic interactions that are mediated by the cations. This article reports structural, property, and bonding details of this series, and some ramifications of adding electrons to a series of isostructural compounds that included the valence-precise La_3In_5. These compounds present a clearly different regime than do many more molecular systems wherein such metallic characteristics would be quite foreign, and free electrons would normally be expected to reduce or "open up" homoatomic bonds.

(1) This research was supported by the Office of the Basic Energy Sciences, Materials Sciences Division, U.S. Department of Energy (DOE). The Ames Laboratory is operated for DOE by Iowa State University under Contract No. W-7405-Eng-82.

(2) (a) Zintl, E. *Angew. Chem.* **1939**, *52*, 1. (b) Klemm, W.; Bussmann, E. *Z. Anorg. Allg. Chem.* **1963**, *319*, 297. (c) Schäfer, H. *Annu. Rev. Mater. Chem.* **1985**, *15*, 1;. (d) Wade, K. *Adv. Inorg. Chem. Radiochem.* **1976**, *18*, 1.

(3) Cromer, D. *Acta Crystallogr.* **1976**, *B32*, 1930.

(4) Zhao, J.-T.; Corbett, J. D. *Inorg. Chem.* **1995**, *34*, 378.

(5) Corbett, J. D. In *Chemistry, Structure and Bonding in Zintl Phases and Ions*; Kauzlarich, S., Ed.; VCH: New York, 1996; Chapter 3.

10.1021/ic010804v CCC: $20.00
Published on Web 11/15/2001

Experimental Section

The general techniques utilized welded Ta containers, glovebox operations, and Guinier powder diffraction, as have been described earlier.[6,7] An improved method for sample mounting for powder pattern measurements was employed. Samples were held between two sheets of aluminized polyester film by means of a thin centered film of vacuum grease that also sealed the outer edge of the sheets to prevent decomposition of the air-sensitive products.[7] Thus the appearance of broad patterns of Sn or Pb metals in the patterns from subsequent accidental oxidation of the sample surface was greatly reduced over that previously achieved with cellophane tape mounting. All operations were carried out in N_2- or He-filled gloveboxes.

Syntheses. The synthesis of Sr_3Sn_5 was carried out by mixing stoichiometric amounts of strontium (Aesar, distilled, 99.8%) and tin (Aesar, 99.99%), allowing these to prereact at 900 °C and then quenching and equilibrating the material at 570 °C for 3 weeks. The product was brittle and gray. An X-ray powder pattern of the product could be entirely indexed on the basis of the Pu_3Pd_5 structure type. The composition of this phase, 37.5 a/o Sr, falls close to the boundary between two earlier studies of the Sr−Sn system, 35%, but neither saw evidence for it.[8] It is furthermore not clear whether otherwise assigned isothermal events at 580−598° or 820 °C in this region might be the peritectic decomposition or melting temperature for Sr_3Sn_5, although the higher value seems more likely.

The synthesis of Ba_3Pb_5 was similarly carried out by direct fusion of stoichiometric amounts of barium (Aesar distilled, 99.8%) and lead (Aesar, 99.9999%) at 1000 °C for 2 h, after which the mixture was cooled at 6 °C/h to 550 °C and held for 2 h. The X-ray powder pattern likewise revealed only the Pu_3Pd_5-type product, and the refined lattice constants were in good agreement with those reported by Bruzzone and co-workers.[9] The La_3Sn_5 was also made by direct combination of lanthanum (Ames Lab, 99.999%) and tin at 1300 °C, where it was held for 12 h and then slowly cooled to room temperature over 2 days. Its X-ray powder pattern revealed the expected Pu_3Pd_5-type pattern in an apparent quantitative yield (>95%), and the lattice dimensions are close to those reported earlier for a phase thought to be related to Pu_3Pd_5.[10] More importantly, intensity distributions in all three patterns were in excellent agreement with those calculated on the basis of the refined structural data (below).

Hydride errors can be particularly serious with many commercial alkaline-earth metals.[11] The absence of significant hydride in what we identify as Sr_3Sn_5 and Ba_3Pb_5 was ensured by production of materials with the same dimensions in each case whether these were made (a) with a SrH_2 or BaH_2 source, (b) when a dynamic vacuum was applied to the Sr−Sn system in Ta at temperature to remove H, or (c) carefully sublimed Ba was used in that synthesis.

Attempts to prepare a number of other isotypic, cation-precise or excess electron phases with the same anions were not successful, i.e., KSr_2Sn_5, $RbSr_2Sn_5$, Rb_2SrSn_5, Sr_3Sn_4As, Sr_3Sn_4Ga, $CsSr_2Sn_5$, Cs_2SrSn_5, Cs_2BaPb_5, and Rb_2BaPb_5. Antimony analogues were not found, and cation-richer phases such as $Cs_3La_2In_5$ that might provide better separation of In_5^{9-} units were not achieved either. It was possible, however, to mix alkaline-earth with rare-earth metal cations to prepare other isotypic phases that presumably had 2−5 electrons in excess of the expected closed-shell values, e.g., $YSr_2Sn_5 + 3e$. It was also possible to substitute up to ~20% Ga for Sn2 in $La_3Sn_{4.6}Ga_{0.4}$.

X-ray Diffraction. Powder diffraction data obtained by an Enraf-Nonius Guinier camera and Cu Kα1 radiation were used for phase identification. The films were usually first compared semiquantitatively with the patterns calculated for phases with known structures. The compositions of mixed products were estimated visually from relative powder pattern intensities, considering unit cell contents as well. The cell parameters listed in Table 1 were obtained by least squares refinement of measured and indexed 2θ values utilizing NIST silicon as an internal standard.

Table 1. Cell Parameters (Å, Å^3) of Orthorhombic Pu_3Pd_5-Type Phases[a]

compound	*a*	*b*	*c*	*V*
La_3In_5[b]	10.345(4)	8.424(6)	10.643(6)	927(2)
Sr_3Sn_5	10.644(2)	8.588(1)	10.895(2)	995.9(3)
YSr_2Sn_5	10.638(3)	8.581(3)	10.886(4)	993.7(6)
Ba_3Pb_5[c]	11.154(7)	9.049(7)	11.370(5)	1147(1)
La_3Sn_5[d]	10.352(5)	8.290(6)	10.652(2)	914(1)

[a] From Guinier data with Si as an internal standard, 23 °C, $\lambda = 1.540562$ Å. [b] Reference 4. [c] Reference 9 gives 11.148, 9.049, and 11.368 Å, respectively. [d] Reference 10 gives 10.35, 8.29, and 10.63 Å, respectively.

Several small gray crystals of Sr_3Sn_5 were first isolated from a $K_{10}Sr_5Sn_{14}$ reaction mixture, placed into thin-walled capillaries, and checked by Laue photographs. Diffraction data from one specimen (0.25 × 0.13 × 0.15 mm) were collected at room temperature using a Rigaku AFC6 diffractometer with monochromated Mo Kα radiation. Routine indexing of 25 centered reflections gave a C-centered orthorhombic cell. Systematic extinctions led to the selection of space group *Cmcm*, and this, rather than the acentric alternate *Cmc*2, was confirmed in a refinement carried out with the aid of the TEXSAN package.[12] The data were corrected for absorption empirically according to three ψ-scans of strong reflections with different θ values. The final residuals were $R(F)/R_w = 3.6/6.0$ with the largest residual in the ΔF map of 3.6 e/Å, located 0.9 Å from Sn2. Potassium was not found in the structure, as further confirmed by the high-yield syntheses later achieved from stoichiometric reactions in the binary system.

Similarly, small silvery crystals of Ba_3Pb_5 and La_3Sn_5 were mounted into thin-walled capillaries in a glovebox, checked by Laue photographs, and diffractometer data collected from each. The routine indexing and cell reduction procedures indicated C-centered orthorhombic cells for both, and this was verified during collection of a full data set for each. Systematic absences indicated *Cmcm* (No. 63) or $Cmc2_1$ (No. 36), and since a Pu_3Pd_5-type structure was already indicated by the powder diffraction data, the former was chosen. Each data set was corrected for absorption with the aid of ψ-scans of three reflections. Their refinements were uneventful. Anomalous dispersion and secondary extinction were both taken into account. Because of the strong absorption and the inadequate corrections obtained, particularly at higher θ, an additional correction was applied to each data set by means of DIFABS, starting with isotropic atom displacement values and unaveraged intensity data, as recommended.[13] The final residual R/R_w values and largest peaks in the difference maps were as follows: Ba_3Pb_5, 4.2/5.1% and 3.96 e$^-$/Å^3 1.6 Å from Pb2; La_3Sn_5, 3.6/4.1% and 2.8 e$^-$/Å^3 2.1 Å from La2. Most of the published estimates of fractional positional parameters in Ba_3Pb_5 made on the basis of powder diffraction data[9] were off by 0.01−0.02, too much to be useful.

Selected crystallographic and refinement data for the three studies are given in Table 2, and more detailed information and displacement ellipsoid parameters are given in the Supporting Information, Tables S1 and S2. Refined atom positions for the three structures are listed in Table 3. All three are the first structural refinements.

Calculations. Theoretical calculations were made over 216 k-points in the irreducible wedge with the aid of the CAESAR EHTB program of Whangbo et al.[14] Orbital coefficients for all elements and H_{ii} values for the main group atoms were taken from Alvarez.[15] Use of La energy values from the same source in the La_3In_5 and La_3Sn_5 calculations gave

(6) Dong, Z.-C.; Corbett, J. D. *J. Am. Chem. Soc.* **1993**, *115*, 11299.
(7) Kaskel, S.; Corbett, J. D. *Inorg. Chem.* **2000**, *39*, 778.
(8) *Binary Alloy Phase Diagrams*, 2nd ed.; Massalski, T. B., Ed.; ASM International: Materials Park, OH, 1990; p 3400.
(9) Bruzzone, G. L.; Franceschi, E. *J. Less-Common Met.* **1977**, *52*, 211.
(10) Borzone, G.; Borsese, A.; Ferro, R. *Z. Anorg. Allg. Chem.* **1983**, *501*, 199.
(11) (a) Leon-Escamilla, E. A.; Corbett, J. D. *Inorg. Chem.* **2001**, *40*, 1226. (b) Leon-Escamilla, E. A.; Corbett, J. D. *J. Solid State Chem.* **2001**, *159*, 149.
(12) *TEXSAN*, Windows version 1.02; Molecular Structure Corp.: The Woodlands, TX, 1997.
(13) Walker, N.; Stuart, D. *Acta Crystallogr. A* **1983**, *39*, 158.
(14) Ren, J.; Liang, W.; Whangbo, M.-H. *CAESAR*; PrimeColor Software, Inc.: Raleigh, NC, 1998.
(15) Alvarez, A. Tables of Parameters for Extended Hückel Calculations, Parts 1 and 2, Barcelona, Spain, 1987.

Table 2. Selected Details of Data Collection and Structural Refinement for Sr_3Sn_5, Ba_3Pb_5, and La_3Sn_5[a]

	Sr_3Sn_5	Ba_3Pb_5	La_3Sn_5
fw	856.31	1449.47	1018.18
cryst syst, space group, Z	orthorhombic, *Cmcm* (No. 63), 4		
calcd density, g cm^{-3}	5.719	8.391	7.333
absorp coeff μ(Mo Kα, cm^{-1})	281.93	838.34	271.47
R, R_w[b]	0.036, 0.060	0.042, 0.051	0.036, 0.041

[a] Cell dimensions in Table 1. [b] $R = \sum||F_o| - |F_c||/\sum|F_o|$; $R_w = [\sum w(|F_o| - |F_c|)^2/\sum w(F_o)^2]^{1/2}$; $w = \sigma_F^{-2}$.

Table 3. Refined Atomic Positions for Sr_3Sn_5, Ba_3Pb_5, and La_3In_5[a]

	x	y	z	B_{eq}[b]
		Sr_3Sn_5		
Sn1	0	0.0432(2)	0.25	1.20(4)
Sn2	0	0.3134(1)	0.4461(1)	1.24(3)
Sn3	0.1986(1)	0.2907(2)	0.25	1.30(3)
Sr1	0	0.6482(3)	0.25	1.12(5)
Sr2	0.2974(2)	0	0	1.33(3)
		Ba_3Pb_5		
Pb1	0	0.0381(2)	0.25	0.46(7)
Pb2	0	0.3051(2)	0.4460(1)	0.4(1)
Pb3	0.2009(1)	0.2847(2)	0.25	0.57(7)
Ba1	0	0.6361(3)	0.25	0.4(1)
Ba2	0.2069(2)	0	0	0.4(1)
		La_3Sn_5		
Sn1	0	0.0273(2)	0.25	0.81(5)
Sn2	0	0.3198(2)	0.4509(1)	0.76(7)
Sn3	0.2082(1)	0.2848(2)	0.25	0.86(5)
La1	0	0.6371(2)	0.25	0.66(6)
La2	0.2019(1)	0	0	0.73(4)

[a] Site symmetries in A_3M_5 phases (*Cmcm*): M1 4*c mm.*; M2 8*f m..*; M3 8*g ..m*; A1 4*c mm.*; A2 8*e* 2. [b] $B_{eq} = (8/3)\pi^2[U_{11}(aa^*)^2 + U_{22}(bb^*)^2 + U_{33}(cc^*)^2]$.

some nonsensical results, including reverse charge transfer from the anions and to lanthanum. Therefore, the La H_{ii} data were charge-iterated to self-consistency versus In with the aid of a package in the program EHMACC[16] and the charge coefficients from Alvarez.[15] This raised the La values by 2.5 (s) to 3.3 (d) eV. The same was done for Ba_3Pb_5 starting with H_{ii} estimates for Ba from Seo.[17] The H_{ii} values for valence d orbitals on Sr and Ba were obtained following Burdett's method for making multiplicity corrections to the spectroscopic data for neutral atoms.[18,19] All the parameters employed are listed in Table 4.

Property Measurements. Resistivities of Sr_3Sn_5 and La_3Sn_5 were measured by the electrodeless Q method[4] on 66.7 (44.8) mg that had each been sieved to 250−425 μm powder and diluted with chromatographic Al_2O_3. Measurements were made at 34 MHz over 120−240 K. The resistivity of Sr_3Sn_5 extrapolated to 298 K was 11 $\mu\Omega$·cm with a temperature coefficient $[(\delta\rho/\delta T)/\rho]$ of $2.8(3) \times 10^{-2}$ K^{-1}, while La_3Sn_5 yielded 24 $\mu\Omega$·cm at 298 K with about twice the temperature dependence, $5.5(7) \times 10^{-2}$ K^{-1}. The absolute resistivities may be off by a factor of 2 or 3.

Results and Discussion

The present article reports three newly structured members of the Pu_3Pd_5 structure type that are especially novel because of the clear persistence of square pyramidal cluster groups of the elements Sn and Pb in spite of the apparent presence of excess electrons in them. These become more significant chemically when taken together with the prior example of the isotypic La_3In_5.[4] The last had been given the easy assignment as a Zintl phase structurally[21] in response to the evident valence balance between the expected cation oxidation numbers and the nominal closed-shell *nido*-In_5^{9-} anion. The fact that this phase is actually a poor metal will receive further consideration later. The new examples Sr_3Sn_5, Ba_3Pb_5, and La_3Sn_5 are on the same basis 2, 2, and 5 electrons rich, respectively, with regard to valence closure. Most important for the moment is what we can deduce about the bonding in these compounds, including possible or perceptible intercluster bonding interactions as well as, it turns out, significant heteratomic cation−anion bonding or lattice covalence. The fact that the pentatomic anions are not well separated in the presence of a cation:anion ratio of only 3:1 and the relative sizes of the component ions play significant roles in these secondary interactions. The metallic character of La_3In_5 was earlier attributed to intercluster bonding effects.[4] Although we will not consider Madelung energies per se, it must be recognized that the ultimate stability of every particular ion packing must in detail be significantly dependent on this factor as well.

Table 4. Atom Parameters Used for A_3M_5 Extended Hückel Calculations[a]

atom	orbital	ς_{i1}	H_{ii} (eV)	Cl	ς_{i2}	C2
Sr	5s	1.214	−5.69			
	5p	1.214	−3.87			
	4d	3.047	−3.37	0.7492	0.9885	0.5467
Ba	6s	1.21	−5.21			
	6p	1.21	−3.43			
	5d	4.33	−3.99	0.688	1.64	0.595
La	6s	2.14	−5.15			
	6p	2.08	−2.97			
	5d	3.78	−4.90	0.7766	1.380	0.4587
In	5s	1.90	−12.60			
	5p	1.68	−6.19			
Sn	5s	2.12	−16.16			
	5p	1.82	−8.32			
Pb	6s	2.35	−15.70			
	6p	2.06	−8.00			

[a] Data from Alvarez[15] except for H_{ii} for Sr, Ba, and La (see text).

The Structures. The structure description will start with the Sr_3Sn_5 phase as representative of the lot. The previously reported La_3In_5 will be incorporated into the discussion as well, so critical distances in all four phases are listed in Table 5. Near-[100] and -[001] views of the Sr_3Sn_5 (Pu_3Pd_5-type) unit cell are shown in Figure 1, with the Sn_5 units as blue polyhedra and the separate Sr atoms red. The polyanions all have *mm* (C_{2v}) symmetry with the 2-fold axes parallel to $\vec{a}$ and $\vec{b}$ and vertical in the figure. The basal Sn2 and Sn3 atoms do not lie in the same plane, doubtlessly because of the several factors that go into the packing and bonding; the separations between these two atoms parallel to $\vec{b}$ range from 0.17 to 0.29 Å with that in La_3Sn_5 at the upper limit. The ranges of the three independent dimensions within the "square" pyramids, marked at the upper right in Figure 1 for Sr_3Sn_5, reflect this distortion and vary from 0.12 to 0.22 Å, being more nearly proportional for the pairs Sr_3Sn_5 vs Ba_3Pb_5 and La_3In_5 vs La_3Sn_5, larger for the latter in each pair. There are two types of generally longer intercluster distances that are influenced both by the main-group cluster element and the size (and presumably field) of the intervening cations, M2−M2 and M1−M3. The Sn2−Sn2 (base-to-base) separations are marked in Figure 1 with the narrower solid lines, and the usually larger Sn1−Sn3 (base to apex, clearer at the

(16) Charge interations utilized a local variant of the EHMACC suite of programs written and modified by students in R. Hoffmann's group at Cornell University and adapted to the PC by Martin Köckerling.
(17) Seo, D.-K.; Corbett, J. D. *J. Am. Chem. Soc.*, accepted.
(18) Brennan, T. D.; Burdett, J. K. *Inorg. Chem.* **1993**, *32*, 746.
(19) Moore, C. E. *Atomic Energy Levels, National Standard Reference Data Service*, 1971.
(20) Hughbanks, T. In *Inorganometallic Chemistry*; Fehlner, T., Ed.; Plenum Press: New York, 1992; p 291.
(21) Shannon, R. D. *Acta Crystallogr.* **1976**, *32A*, 751.

Table 5. Atom Separations (Å) and Overlap Populations in A_3Tt_5 Compounds (Pu_3Pd_5-Type) (A = Sr, Ba, La; M = In, Sn, Pb; d < 4.1 Å)

atom		Sr_3Sn_3		Ba_3Pb_5		La_3Sn_5		La_3In_5	
A1−M1		3.390(4)	0.26	3.635(4)	0.21	3.234(3)	0.23	3.228(3)	0.23
Al−M2	×2	3.325(2)	0.33	3.497(3)	0.30	3.211(3)	0.29	3.263(3)	0.29
Al−M2	×2	3.580(3)	0.07	3.732(4)	0.07	3.392(2)	0.09	3.449(2)	0.12
Al−M3	×2	3.432(6)	0.32	3.600(3)	0.29	3.259(2)	0.31	3.285(1)	0.31
Al−M3	×2	3.726(9)	0.09	3.889(3)	0.07	3.629(2)	0.10	3.619(2)	0.11
A2−M1	×2	3.492(2)	0.17	3.679(3)	0.13	3.395(2)	0.16	3.400(1)	0.15
A2−M2	×2	3.496(8)	0.15	3.650(3)	0.12	3.416(2)	0.15	3.391(2)	0.17
A2−M2	×2	3.596(7)	0.10	3.766(3)	0.09	3.467(2)	0.11	3.508(1)	0.12
A2−M3	×2	3.426(3)	0.21	3.596(2)	0.17	3.340(2)	0.19	3.330(1)	0.20
A2−M3	×2	3.693(1)	0.06	3.835(2)	0.05	3.562(2)	0.08	3.601(2)	0.10
M1−M2	×2	3.152(3)	0.20	3.284(3)	0.28	3.235(2)	0.16	3.232(2)	0.29
M1−M3	×2	2.997(7)	0.44	3.162(3)	0.45	3.033(2)	0.40	3.147(2)	0.30
M1−M3[a]	×2	3.870(4)	−0.07	4.053(3)	−0.02	3.627(2)	0.04	3.575(2)	0.20
M2−M1		3.152(3)	0.20	3.284(3)	0.28	3.235(2)	0.16	3.232(2)	0.29
M2−M2[a]		3.413(3)	0.23	3.732(4)	0.14	3.165(3)	0.41	3.428(3)	0.29
M2−M3	×2	3.011(2)	0.51	3.166(2)	0.52	3.053(2)	0.43	3.014(1)	0.57
M3−M1		2.997(7)	0.44	3.162(3)	0.45	3.033(2)	0.40	3.147(2)	0.30
M3−M1[a]		3.870(4)	−0.07	4.053(3)	−0.02	3.627(2)	0.04	3.575(2)	0.20
M3−M2	×2	3.011(2)	0.51	3.166(2)	0.52	3.053(2)	0.43	3.014(1)	0.57

[a] Intercluster.

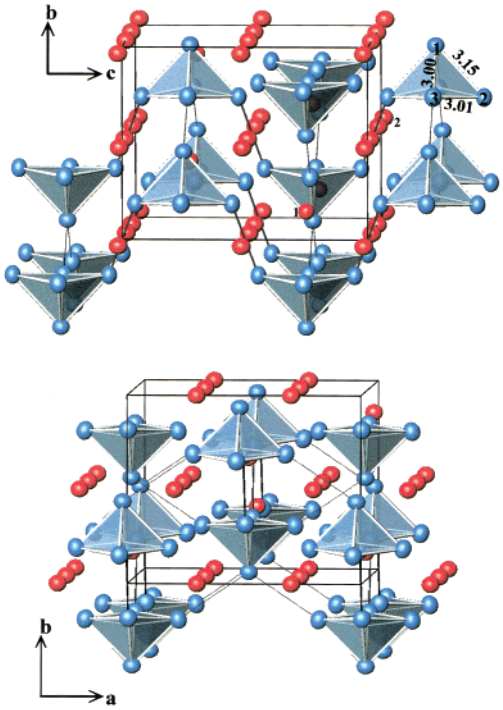

Figure 1. [001] (top) and [100] (bottom) views of the orthorhombic Pu_3Pd_5-type structure of Sr_3Sn_5. The square pyramidal Sn_5 units (C_{2v}) are blue, and the isolated Sr1 and the more populous Sr2 atoms are red. Significant intercluster contacts are shown by light (Sn2−Sn2) and lighter (Sn1−Sn3) black lines, the latter being clearer in the bottom view.

bottom), with lighter lines. These are 0.26 and 0.72 Å longer, respectively, than the largest intracluster distance. The more important intercluster d(M2−M2) values are with one exception longer than all distances within the clusters, by 0.20 Å (La_3In_5) to 0.45 Å (Ba_3Pb_5). In the exceptional La_3Sn_5, bridging by the smaller cations is evidently responsible for an intercluster d(Sn2−Sn2) that is 0.07 Å *shorter* than the opposed elongated intracluster d(Sn1−Sn2), 3.235 Å. But the only significant intercluster bonding via M1−M3 is in La_3In_5, in which the separation is only 0.15 Å longer than d(In2−In2) and comparable in bonding.

Distances between the two independent cations and atoms in the anions are fairly regular. These also allow some comparative measures of anion sizes. The differences in specific d(A−Tt) pairs in Sr_3Sn_5 vs Ba_3Pb_5 are generally close to 0.16 Å, with lead naturally the larger. Since the cation crystal radii (CN8) differ by 0.14 Å,[21] this suggests that the contact radii for the lead atoms in the anion are only slightly greater than for tin. Coincidently, the same numerical differences apply to comparable bond lengths within the two polyanions. In the more important lanthanum salts, the coordination numbers of the cations are generally a little larger for La2 with tin (7−10, depending on cutoff) than for indium, and the distances are correspondingly about 0.1 Å longer (3.28 and 3.44 Å) for A2 vs A1 in both. Because of appreciable conformational changes, distance comparisons for In_5^{9-} vs Sn_5^{4-} (+5e) and the La−M interactions are rather erratic (below).

Bonding. The details of the intercluster and cation−anion bonding need some better basis for interpretation than can be obtained through simple distance tabulations. The two cations in this structure interbridge four to six clusters with seven or eight good A−M interactions each. Because of the limited number of cations and their higher oxidation states, these appear to bring or hold clusters in relatively close proximity compared with internal distances in the Tt_5 units. These somewhat complex interplays are more important to our understanding of these structures and their bonding than just simple descriptions of polyhedra about individual cations. Furthermore, as we have recently noted elsewhere, distances alone may be poor descriptors of bond strength because exterior limitations on distances brought on by atom sizes and packing sometimes produce atom separations that have little to do with bonding, i.e., matrix effects.[22,23]

Thus, a more useful catalog of the pair-wise bonding interactions in these four structures was already included in Table 5, the corresponding Mulliken overlap populations (OP) for each distance from EHTB calculations (below). The larger OP values and the cation bridging effects are best illustrated in Figure 2 for the extreme case of La_3Sn_5. Here "bonds" between atoms are shown with line widths proportional to OP, black for Sn−Sn and orange for La−Sn. (Remember that these are not intercomparable because of overlap integrals that are included. Also, the use of Hamiltonian COHP values, which better

(22) Maggard, P. A.; Corbett, J. D. *J. Am. Chem. Soc.*, **2000**, *122*, 832 and references therein.
(23) Herle, P. S.; Corbett, J. D. *Inorg. Chem.* **2001**, *40*, 1858.

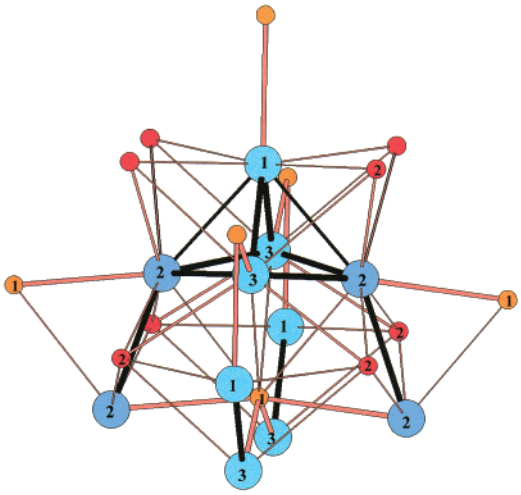

Figure 2. A single cluster in La_3Sn_5 (blue atoms, with Sn2 darker) plus parts of neighboring clusters to which it is bonded and the cations that interconnect these, La1 (orange) and La2 (red). Line widths for the interconnections are proportional to overlap populations for the separate sets, Sn−Sn, black, and La−Sn, orange-red.

approximate bond energies, would underweight the listed heteroatomic values.[24]) Figure 2 contains one complete cluster and the parts of four neighboring clusters (blue, with Sn2 darker) that have significant intercluster interactions therewith plus the bridging lanthanum atoms (La1 orange, La2 red) that are involved with these tin atoms. (The whole cluster is equivalent to that at the upper left in Figure 1.) Particularly striking here is the strength (OP) of the Sn2 − Sn2 intercluster bonding in La_3Sn_5, in which each pair of Sn2 atoms is bridged by two La1 and two La2. A substantial role of La1 in strong interactions with four different clusters is also seen at the bottom center. (There are, of course, many other packing components that lead to this structural result.)

The DOS (densities of states) and COOP (crystal orbital overlap populations) output from extended Hückel calculations give better overall insights as to the nature of, and the bonding in, these unusual compounds. They also offer a critical look at both the easy assumption of a Zintl phase classification for La_3In_5 and the question as to whether the new members of the electron-rich series reported here somehow fit into a different scheme. The existence of a fairly uniform and seemingly dominant heteroatomic lattice covalency is the most striking revelation.

Continuing with Sr_3Sn_5, the DOS curve (solid) plus the PDOS projections of Sn (dotted), Sr s,p (dashed), and Sr d (dash−dot) contributions are shown in Figure 3, left. The broad intracluster valence peaks for Sn centered around −10 eV also involve some Sr (covalent) contributions. The low DOS at about −7.8 eV corresponds to filling of the classic Sn_5^{4-} bonding orbitals, 24 e^- (and certainly not that appropriate to a 26-electron *arachno*-Sn_5^{6-} [25]), whereas appreciable Sn 4p and, increasingly, Sr 4d states are involved above there. The latter do not reach a maximum until about 4 eV about E_F (−6.34 eV in this approximation), in contrast to what we shall see below with lanthanum cations. (The Sn 5s is dominant below about −13 eV. Note its importance according to intracluster COOP data, showing that simple "s cores" are not appropriate to this picture. On the other hand, the Sr 5s is generally not important anywhere.)

(24) Glassey, W. V.; Hoffmann, R. *J. Chem. Phys.* **2000**, *113*, 1698.
(25) Fässler, T. F.; Hoffmann, S. *Z. Kristallogr.* **1999**, *214*, 722.

A clearer understanding of bonding in Sr_3Sn_5 comes from plots of the COOP data: overlap-weighted (Mulliken) bond populations, Figure 3 right, in which the Sn−Sn results are separated into intra- (dotted) and intercluster (dashed) portions. The former component shows a switch from bonding to antibonding contributions just at the point at which the classical valence shell is filled, as it should. The individual types of intercluster interactions (not shown) are slightly bonding for Sn2−Sn2 and antibonding for Sn1−Sn3 near −8 eV, but both are small. There is clearly nothing significant in the way of a Sr−Sr band (dash−dot curve) compared with the evidently dominant effect of heteroatomic Sr−Sn bonding (solid line) that occurs throughout what could be called the valence band and around and above E_F. Plots of the individual Sr_i−Sn_j functions therein (not shown) indicate fairly uniform contributions across all of the bands. The clear bonding peak near −7 eV arises mainly from most of the Sr−Sn pairs that have appreciable overlap populations, Table 5. The charge distributions (from atom populations) are about +1.1 for Sr1, and +1.4 for Sr2 with its higher CN and longer *d*(Sr−Sn). These would be larger were the Mulliken approximation not to divide bond populations equally.

The bottom line is that a Sn_5^{4-} anion does not exist in any isolated sense in Sr_3Sn_5 because of both the extra electrons and the overarching lattice band (covalency) from multiple and strong Sr−Sn interactions. Nonetheless, that well-bonded closed-shell cluster anion persists in this somewhat complex lattice. There is no a priori reason that would preclude the existence of this electride salt either, but its prediction (or not) has much to do with the effects of efficient packing of the extra cation.

The comparable data for Ba_3Pb_5 are not sufficiently different to detail. The heteroatomic distances and bond populations are naturally longer and less, respectively, whereas Pb−Pb populations in the nominal anions are comparable. Expectations for Ba 5d energy (Table 4) put this much closer to its 6s level (∼1.2 eV difference vs 2.6 eV for Sr 4d vs 5s). Shapes of the DOS and COOP curves are very similar to those for Sr_3Sn_5.

Retention of the nominal Sn_5^{4-} anions but a switch to lanthanum cations increases the magnitude of several effects just described for strontium. This change increases the formal excess electron count to five per formula unit, but the major effects seem to be associated with the smaller size and higher charge of La^{3+} (1.30 Å vs 1.40 Å for Sr^{2+} and 1.56 Å for Ba^{2+} for CN8[19]) and the greater proximity of the La 5d valence orbitals, all of which seem to increase what we designate as the lattice covalency substantially. The size decrease naturally increases the intercluster interactions significantly via the tighter interbridging of clusters by the cations; see Sr_3Sn_5 in Figure 2. Figure 4 illustrates the theory results, starting with the DOS for La_3Sn_5 together with PDOS for Sn (dotted) and La (dashed). The minimum in the Sn contributions near −7.8 eV corresponds to the (not quite) closed shell for internal bonding in the square pyramids, whereas both Sn and, increasingly, La are involved in the bonding up to E_F, −5.68 eV. The latter are substantially all La 5d, whereas La 6s is not appreciably involved below ∼−3.5 eV by these approximations. The COOP results (Figure 4, right) can now be anticipated: a more emphatic and wider involvement of the lattice covalency (solid line), from the start of the Sn p band and extending to appreciably higher energies. The antibonding Sn−Sn state components over the last 5e^- below E_F are principally intracluster, with the intercluster contributions being slightly antibonding for Sn2−Sn2 (3.16 Å) and distinctly so for Sn1−Sn3 (3.63 Å) just below E_F. The charges on the La ions in this approximation are each about

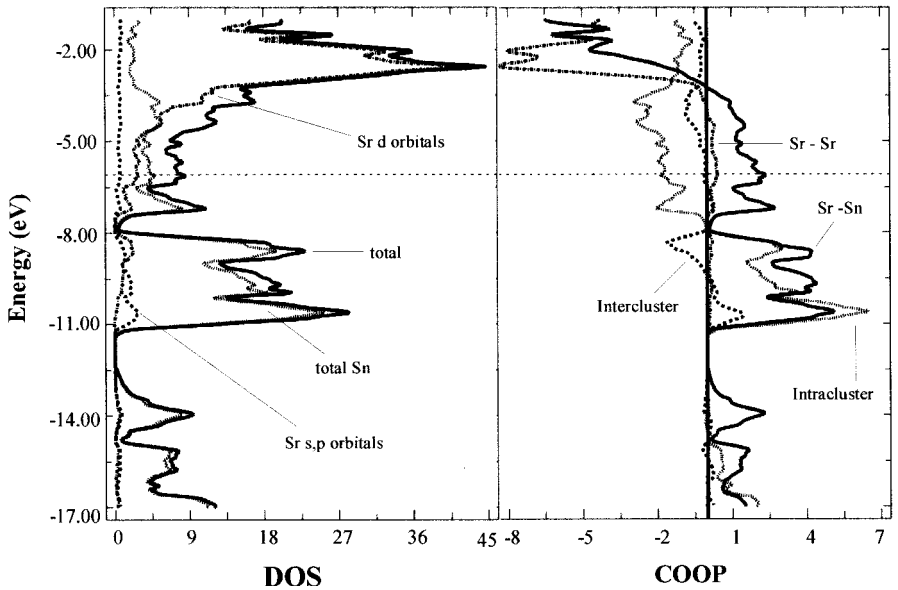

Figure 3. EHTB calculation results for Sr_3Sn_5. Densities of states (DOS) (left) include projections of partial values for Sn (dotted), Sr s,p (dashed), and Sr d (dash−dot). The COOP results on the right show total Sr−Sn (solid), intracluster Sn−Sn (dotted), intercluster Sn−Sn (dashed), and Sr−Sr (dash−dot).

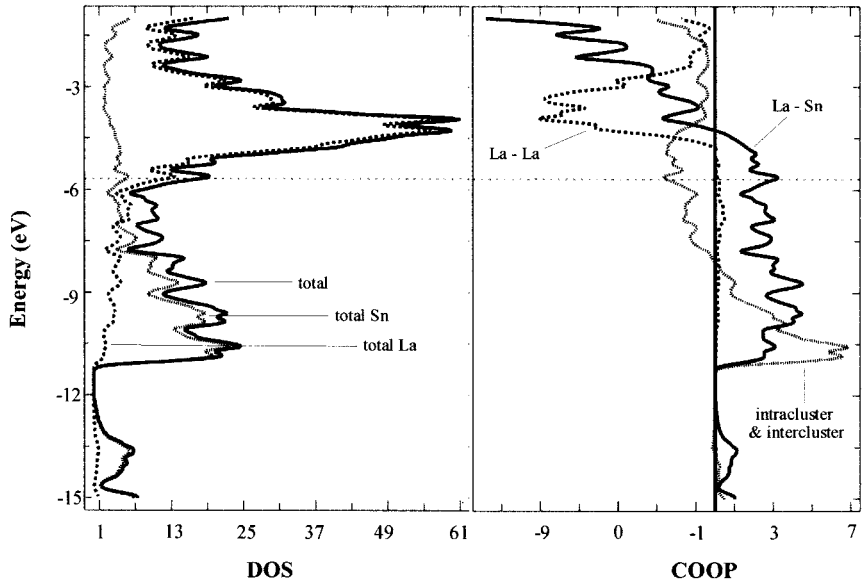

Figure 4. DOS and COOP results for La_3Sn_5. The former on the left represent total (solid), Sn (dotted), and La (dashed) components. In the COOP data on the right, the solid line represents the dominant La−Sn bonding, the dotted, total Sn−Sn, and the dashed, total La−La.

0.1 less than found in Sr_3Sn_5, in parallel with the greater evident La−Sn bonding and in contrast to their higher oxidation state.

We can now return to the original member La_3In_5, for which oxidation state and cluster valence rules predict it to be a valence (Zintl) phase according to the simplest, structural viewpoint. This is in reality a poor assignment, basically because of the strong La−In covalency. Differences in the comparison with La_3Sn_5 include In states that lie 3.6 (s) and 2.1 (p) eV higher than for Sn, and La−M distances and OP values that are ∼0.01 Å larger and very similar, respectively, for In relative to Sn. Changes in packing and bonding lead to a significant intracluster OP for In1−In3 although the separation is only 0.05 Å shorter than for Sn1−Sn3, whereas In2−In2 lengthens by 0.26 Å relative to Sn2−Sn2 but the OP decreases only modestly. Projection of the In and La orbital contributions in DOS, Figure 5, shows a familiar pattern except that there are closer to three valence bands, but there is no sign of a gap near E_F for In_5^{9-}. Large lanthanum contributions are spread throughout the upper pseudo-valence band, and this is seen clearly in the dominance of La−In bonding in the COOP data, the solid line in the right part of Figure 5. The intracluster In−In bonding is again optimized at E_F, the closed shell for the isolated In_5^{9-} anion, but the total In−In bonding is optimal somewhat lower because the now-shorter intercluster In1−In3 (Figure 2, Table 5) is substantially antibonding around E_F (not shown). Both intercluster interactions (dashed line) make comparable and mainly bonding contributions at lower energies.

We have, by the way, not considered the isotypic β-Y_3In_5[4] here because the smaller cation results in markedly shorter intercluster distance relative to those within the In_5 units, and we expect that these as well as appreciably greater lattice covalence will make this even further from a classical Zintl phase.

The collective results above provide useful information and education on the all-too-easy Zintl phase classification afforded by the simplest bonding ideas. These seem to work fairly well

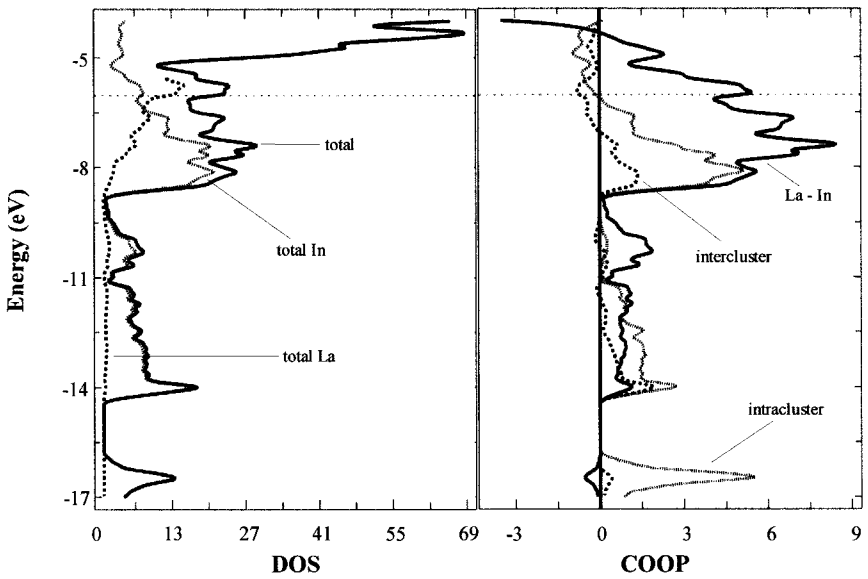

Figure 5. The DOS and COOP data for La_3In_5 with solid, dotted, and dashed curves in the DOS showing total and partial In and La data, respectively. In the COOP results, the solid line gives the La−In data, and the dotted and dashed, In−In intra- and intercluster values, respectively.

for alkali-metal−tetrel and −pnictide examples, which are often semiconductors when resistivities are measured (which is fairly seldom). On the other hand, most valence-precise cluster phases for alkali-metal−triel phases are found to be metallic, although at the same time often diamagnetic, probably because of the unusual diamagnetic components that contribute to the magnetic susceptibilities for these heavy elements.[5] Metallicity in the triel examples may arise in general because of the virtual disappearance of an electronic gap, reflecting the lower electron affinities of the triel elements. We have also recently noted a significant covalence entering into alkaline-earth metal−triel phases with network structures according to theoretical considerations.[17] The greater Madelung energies in most of the latter salts are apparently an increasingly important factor, and good accommodation of the higher field cations becomes more important as well. In addition, achievement of formal closed-shell electronic structures for the alkaline-earth metal examples appears to be less frequent with these higher charged cations, most being slightly electron deficient. It would appear that the Madelung energy must play an important role in the stabilities of the cation and electron-rich compounds considered here as well, the great numbers of and high effective charges on the extra cation in Sr_3Sn_5 etc. being significant relative to the unknown Sr_2Sn_5. Of course, much more subtle factors of alternate phase stability also come into play here, and treatment of the delocalized electrons in a Madelung energy sense is problematic.

A novel variation of these mixed salt−metal characteristics is found in $Ca_5In_9Sn_6$.[26] Here close packed metallic layers of $AuCu_3$ and Ni_3Sn types alternate with Zintl layers containing In_3^{5-} and Ca^{2+}.

There is another meaningful chemical viewpoint regarding the electron-rich phases, evidently first expressed by Nesper.[27,28] We find here and many places elsewhere well-segregated clusters whose compositions, configurations, and evident formal charges agree well with classic Wade's rule or more theoretical MO descriptions, giving us useful ways to understand and correlate these features. Some of these may coincidentally also be metallic, a property of the least bound electrons, whereas the clusters that chemists readily see represent strong interactions of more tightly bound electrons. In the present work we see that such units and the chemistry they represent persist in the presence of stoichiometrically excess electrons. This seems important. Nesper has aptly likened this to structures that may be found in the oceans, buried by the sea: conduction electrons in this case. Things are just harder to sort out under these circumstances.

Finally, to dispense with another supposed problem, the lack of further reduction of the Tt_5^{4-} anions in these metallic Zintl phases:[28] Most other possibilities are less reduced (Tt_4^{4-}, Tt_9^{4-}, etc.) except for formal isolated monoanions Tt^{4-} found in few examples in the presence of dipositive or more highly charged cations, e.g., Ca_2Sn (Co_2Si) and Ca_5Ge_3 (Cr_5B_3). We believe that the question is just not that simple in dense polar solids in which strong interactions and packing are much more important. Quantitative explanations of relative phase stabilities in the latter are not possible even when you know the alternate structure types, and they are impossible when you do not. Exploratory synthesis is still essential to progress.

Acknowledgment. We are indebted to D.-K. Seo for help and advice on the calculations and their interpretations.

Note Added in Proof. A study (ref 25) of Sr_3Sn_5 and other alkaline-earth metal tetrelide analogues by Zürcher and coworkers has now appeared (ref 29). Syntheses and structures of Sr_3Sn_5 and Ba_3Pb_5 were also reported. Extended Hückel, LMTO, and ELF investigations started with an *arachno*-Tt_5^{6-} model derived from the pentagonal bipyramid. The results are along the line of our conclusions in that the HOMO for the Tt_5^{6-} model was found to be antibonding and the two electrons therefore delocalized. Reasons for the cluster distortion were also found.

Supporting Information Available: Tables of additional crystallographic and refinement information and anisotropic displacement parameters for the three structures. This material is available free of charge via the Internet at http://pubs.acs.org.

IC010804V

(26) Xu, Z.; Guloy, A. M. *J. Am. Chem. Soc.* **1998**, *120*, 7349.
(27) Nesper R. *Prog. Solid State Chem.* **1990**, *20*, 1.
(28) A "metallic Zintl phase" appelation was evidently first applied to "valence" compounds containing excess electrons.[27] We use it in the same sense here, this seeming to be preferable to its application to valence-precise phases that are coincidentally metallic.[5]
(29) Zürcher, F.; Nesper, R.; Hoffmann, S.; Fässler, T. F. *Z. Anorg. Allg. Chem.* **2001**, *627*, 2211.